Numerical study of the air conditioning of a room in the city of Mamou (Guinea) by a two-phase thermosiphon loop

ABSTRACT

This document presents a numerical study of the air-conditioning of a room by a two-phase thermosiphon loop in climatic conditions of the Mamou region (Guinea). The room is composed of a roof of rectangular shape and a cabin part assimilated to a parallelepiped. In addition, the air-conditioning unit which operates with methanol is composed of an evaporator, a condenser, a riser and a downcomer. The heat transfer modeling governing the habitat model and the air conditioning loop is based on the nodal method. The equations are solved by the implicit finite difference method. Thus, the numerical resolution allowed to determine the influence of the parameters on the model. The results from the study, shows that the room temperature can be maintained by the air conditioner at a value of 26 °C. This is possible even during the extreme heat of the daytime period. The variation of parameters such as temperatures, wall thickness, incident solar flux, air exchange and evaporator surface also shows their behaviour in the air-conditioned environment. It turns out that they have a significant impact on the operation of the air conditioner and on the temperature of the conditioned room. A low wall thickness or a high air exchange rate contributes to the increase of the temperature of the air-conditioned room.

Keywords: Modelling, optimisation, passive air conditioning, two-phase thermosiphon loop

1. INTRODUCTION

In recent years, the trend of increasing demand for air conditioning, especially in buildings, has been observed in many countries. However, even if the figures vary from one country to another, it is argued that on a global scale, about 40% of the total building energy is consumed for space heating and cooling applications in residential and commercial buildings [1]. In most regions of Guinea like Mamou, the urbanization rate is increasing daily. Moreover, there is no thermal and energy regulation in this sector. Most often these buildings are poorly oriented and are subject to climatic effects (sunshine, wind, etc.) which can be severe and difficult to control. In addition to these constraints, global warming and the heat island effect combined with poor building design [2] contribute greatly to the increase in internal temperatures of the premises and require the integration of an efficient air conditioning system without energy consumption. At the same time, in this country the majority of the population lives in inadequate and overcrowded houses, sometimes with or without electricity. The demand for electricity far exceeds the supply due to population growth and urbanization rate, thus causing malfunctioning of electrical installations. Moreover, only 18% of the national population has access to electricity, which is among the lowest rates in the sub-region [3]. However, electricity is the main source of energy for the operation of active air conditioning systems [4]. Hence the need to

develop passive cooling techniques that reduce the energy consumption of buildings, protect the environment and the ecosystem and provide a satisfactory level of comfort to cope with this crisis. Two-phase thermosyphon loop air conditioning is one of the technologies that can achieve significant energy savings and carbon emission reductions. This system is a self-contained device that works with a temperature difference. A two-phase air-conditioning loop is able to dissipate high thermal power with a very low quantity of fluid which is interesting when the working fluid becomes expensive or harmful for the environment. In addition to these advantages, this thermosyphon system is less bulky, less expensive and its application as a passive cooling loop offers the advantage of operating without any mechanical pumps and without noise [5][6]. A diphase cooling loop is mainly composed of an evaporator which represents the hot source to dissipate heat contained in a room and a condenser which represents the cold source and which allows to liquefy the heat transfer fluid. These two components are connected by pipes: a steam pipe and a liquid pipe. In order to ensure the gravity operation of the loop, the condenser must be placed above the evaporator [7]. Several researchers have done experimental and numerical studies on the thermal performance, optimum filling ratio, heat transfer methods and operating conditions of the two-phase thermosiphon loop in recent years. Chehade, A. et al. [8], made a modeling and experimental study of a thermosiphon loop intended to cool a telecommunication cabinet. The test was done with different working fluids. The system is studied to define an optimal pipe diameter (liquid and steam) and the effect of ambient temperature on the mass flow rate and pressure drop of the fluid. The results show that the best working fluid is the one that gives a lower loop response time and thermal resistance. Indeed, increasing the pipe diameters by 0.012 m and 0.014 m would be a key factor in improving the system efficiency. On the other hand, increasing the outdoor ambient temperature negatively affects the cooling performance by increasing the mass flow in the loop and decreasing the evaporator pressure drop. Their prototype does not require a pump for the circulation of the heat transfer fluid. The equipment housings are placed in the center of the cabinet with the heat adjusted by means of an autotransformer. Cao, H., et al. [9] focused through an experimental study and numerical simulation to investigate the height of the downcomer refrigerant. The results indicated that a high refrigerant column height would occupy part of the condenser space and reduce the performance of the two-phase thermosiphon loop. Zhang, P., et al. [10] did a modeling and experimentation of a two-phase thermosiphon loop in which the downcomer can be partially or completely filled with liquid. In their study, it is shown that when the temperature difference and the refrigerant charge are very low then the downcomer is partially filled with liquid and increasing these would increase and then decrease the heat transfer rate. Khodabandeh, R. et al. [11] observed instabilities of different nature which appeared at low or very high heat fluxes and worsen with large diameter of the evaporator pipes. Tong, Z. et al. [12] experimentally tested the effects of fill rate on the operating stability of a loop using R744 as the working fluid. It is found that, the optimal fill rate to achieve the loop's ability to transfer maximum heat is 100%. Under the fill rate higher or lower than this value, the ability of the loop to transfer heat will be decreased. In another study [13], the same authors experimented with a two-phase thermosyphon loop using R744 and R22 under different heat transfer rates from 1 to 4 kW. In this study the thermal performance and resistance for cooling a data center are examined. It is found that R744 offers better

cooling performance and that the thermal resistance of R744 is 22-25% lower than that of R22. In this paper, we evaluate through a numerical study the heat transfer in a room integrating a two-phase thermosiphon loop for a dry and humid tropical climate. To do this, we propose a mathematical model based on the nodal method that describes the operation of the air conditioning loop and the habitat. The model concerns the heat transfers of the room and the air conditioning loop composed of an evaporator, a condenser, a riser and a downcomer. Then we will make the coupling between the habitat and the air conditioning unit in order to observe the impact of the air conditioner on the temperature profile of the internal air of the room. Thus, we observe in the time, the evolution of the various parameters in the air-conditioned room. Finally, we present the influence of some input parameters in order to evaluate their impact on the air conditioning system including the thermal comfort of the habitat taking into account the climatic conditions of the city of Mamou.

2. METHODOLOGY AND MATERIALS

2.1 Presentation of the study area

Mamou, the study area is located 270 km from the capital Conakry, in the south of the central massif of Fouta-Djallon between 10° 22.53' North latitude and 12° 5.48' West longitude. The prefecture of Mamou covers an area of 8674.32 km² with an altitude of 720 m above sea level. The urban commune is limited to the East by the rural communes of Soyah and Dounet, to the West by Konkouré, to the North by Boulliwel and Tolo and to the South by Konkouré and Soyah (Fig.1.). The relief and altitude in Fouta are the essential factors of the climate. Like middle Guinea in general, Mamou has a tropical (or foutanian) climate, characterized by two alternating seasons, a dry season (November to April) and a rainy season (May to October). The harmattan is felt in the dry season and the hygrometric degree of the air easily falls below 45%. Rainfall is very abundant with an average annual rainfall of 2,087 mm. Average monthly temperatures range from 21° to 28°C. The highest maximum temperatures are observed in March and April with an average temperature that sometimes reaches 37°C while the lowest minimum temperatures of about 11°C on average are recorded in December. As for the winds, apart from the harmattan and the monsoon which are dominant on the ground, the mountain and valley breezes blow regularly. The relief of the urban commune is uneven, consisting of plateaus forming the beginning of the Fouta Djallon massif, which makes it difficult to move between the different districts. The vegetation of the commune is very favoured. It is essentially made up of bamboos, cheese trees, cailcédrat, baobab and others. In addition, there is a wide range of fruit trees: Mango, Avocado, Papaya, Citrus, etc. There are also classified forests in Tyéwel, Sérè, Koumi, Diarabaka and Tambassa.

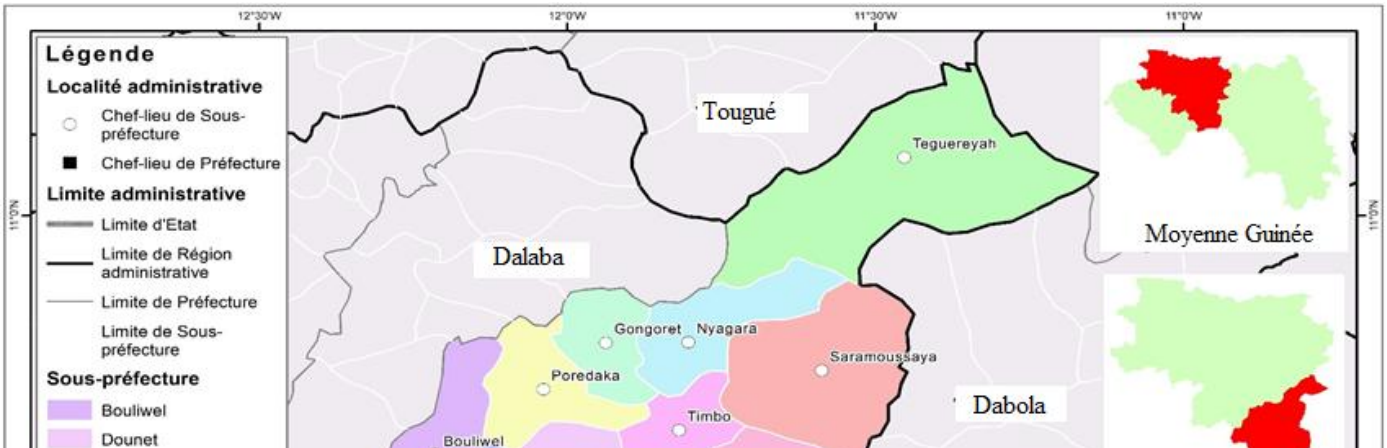

Fig. 1. Location of the study area.

2.2 Description of the physical model

The habitat model selected for this study is a classic habitat typical of Guinea. It is composed of two parts: a roof and a living area. The roof is rectangular in shape, sloping towards the south at an angle of 30° to the horizontal and 0.5 m high. It is covered with galvanized steel sheets of a thickness of about 5 mm and a high thermal conductivity of about 50 W/m². The roof is separated from the passenger compartment by a false ceiling made of wooden counter plates which acts as insulation as shown in Fig. 2. The cabin is a parallelepiped of 4x3x3 m with a surface of 12 m². The wall is 15 cm thick and is built with clay bricks and concrete floor. The selected habitat model is equipped with an air conditioning loop composed of an evaporator, a condenser, a riser and a downcomer. The evaporator is located in the room to be air-conditioned and the condenser outside the room (Fig. 2). The pipes are insulated in such a way that the heat loss of the heat transfer medium can be neglected. Copper is used as the material for the cooling loop. The thermo-physical properties of the materials for the house and the cooling loop are presented in Table 1.

Materials	**Density** $\rho\ (kg/m^3)$	**Heat capacity** $c_p\ (J/kg.K)$	**Thermal conductivity** $\lambda\ (W/m.K)$
Habitat			
BTC	1850	1000	1.150
Galvanized steel sheets	7800	450	50
False ceiling in plywood	800	1600	0.24
Concrete	2300	100	0.8
The air conditioning loop			
Air	1.16	1006	0.0261
Copper	8900	380	380

Methanol (liquid)	786	4390	
Methanol (Steam)	0.218	1400	

Table 1. Thermo-physical properties of materials.

2.3 Working principle of the model

The incident solar flux reaches the roof and the walls of the house. Due to the effect of the atmosphere and the incident solar flux, the various components of the house (the galvanized steel roof, wall, false ceiling, etc.) absorb heat during the day. This heat is transmitted to the indoor air of the house by conduction, radiation and convection through the openings. Thus, the temperature of the indoor air increases throughout the day. The different modes of heat transfer are illustrated in Fig. 2. As for the air-conditioning loop, it operates with methanol as the heat transfer fluid. The refrigerant absorbs heat from the environment to be cooled and evaporates in the evaporator. The refrigerant vapour rises in the riser under the action of buoyancy forces generated by the differences in density of this fluid in the riser and the downcomer. It condenses in the condenser, releasing its latent heat of condensation. The condensate flows by gravity into the downcomer and returns to the evaporator.

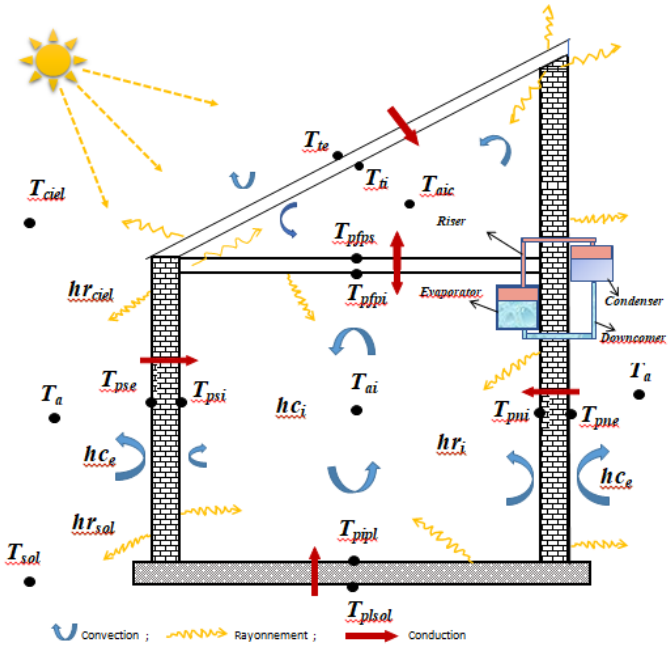

Fig. 2. Different modes of heat transfer in the home

2.4 Mathematical formulation

2.4.1 Assumptions

- Heat transfer is unidirectional;
- The temperature distribution on the inner and outer walls is uniform,
- The thermo-physical properties of materials are constant
- All the evaporated mass is condensed,
- One-dimensional fluid flow;
- Steam is an ideal gas;
- Boiling occurs at the evaporator;
- Condensation in the film occurs at the condenser.

2.4.2 Model equations

The heat transfer equations governing the model are based on the nodal method. Then we establish a thermal balance based on the analogy between thermal and electrical transfers on each of the elements considered. Thus, we consider each node (i) an independent element from the others and we apply the law of conservation of energy. The heat transfer balance equation is written by [14]:

$$m_i Cp_i \left(\frac{\partial \mathrm{T_i}}{\partial \mathrm{t}} \right) = \alpha_i G_i + \sum_i h_{xij} S_i \left(T_j - T_i \right) + \Phi_i \quad (1)$$

2.4.3 Heat transfer balance equation of the habitat

The heat transfer balance equation at the air level of the living area is written by :

$$\rho_{ai} V_{ai} c_{p,ai} \left(\frac{\partial T_{ai}}{\partial t} \right) = \sum_{j=1} hc_{j,pi} S_{j,pi} \left(T_j - T_{ai} \right) + hc_{evap} S_{evap} \left(T_{evap} - T_{ai} \right) + \phi_{ra} \quad (2)$$

With : $\phi_{ra} = 0.34 NV \left(T_a - T_{ai} \right)$

The heat transfer balance equation for all the external walls of the house is written as :

$$\frac{\rho_M V_M c_{p,M}}{S_{pe}} \left(\frac{\partial T_{pe}}{\partial t} \right) = \alpha_p G_p + \frac{\lambda_M}{e_M} \left(T_{pi} - T_{pe} \right) + hc_e \left(T_a - T_{pe} \right) + hr_{sky,pe} \left(T_{sky} - T_{pe} \right) + hr_{soil,pe} \left(T_{soil} - T_{pe} \right) \quad (3)$$

The heat transfer balance equation for all the internal walls of the house is written as :

$$\frac{\rho_M V_M c_{p,M}}{S_{pi}} \left(\frac{\partial T_{pi}}{\partial t} \right) = \frac{\lambda_M}{e_M} \left(T_{pe} - T_{pi} \right) + hc_i \left(T_{ai} - T_{pi} \right) + \sum_{j=1} hr_{j,pi} \left(T_j - T_{pi} \right) \quad (4)$$

2.4.4 Heat transfer balance equation of the air conditioning loop

The heat transfer balance equation of the internal walls of the evaporator and the condenser is determined by :

$$\frac{mc_p}{S} \left(\frac{\partial T_{pi}}{\partial t} \right) = \frac{\lambda_M}{e_M} \left(T_{pe} - T_{pi} \right) + hc \left(T_f - T_{pi} \right) \quad (5)$$

Heat transfer balance equation at the external walls

- At the evaporator

$$\frac{mc_p}{S} \left(\frac{\partial T_{pe}}{\partial t} \right) = hc \left(T_a - T_{pe} \right) + \frac{\lambda_M}{e_M} \left(T_{pi} - T_{pe} \right) \quad (6)$$

- At the condenser

$$\frac{mc_p}{S}\left(\frac{\partial T_{pe}}{\partial t}\right)=\alpha_p G_p+hc\left(T_a-T_{pe}\right)+\frac{\lambda_M}{e_M}\left(T_{pi}-T_{pe}\right)+hr_{soil}\left(T_{soil}-T_{pe}\right)+hr_{sky}\left(T_{sky}-T_{pe}\right) \quad (7)$$

Heat transfer balance equation at the fluid level

- At the evaporator

$$m_f c_{pf}\left(\frac{\partial T_f}{\partial t}\right)=\sum_{j=1} hc_j S_j\left(T_{j,pi}-T_f\right)-\dot{m}h_{fg} \quad (8)$$

The flow rate is calculated by : $\dot{m}=S\beta_m\left[w_{vs}\left(T_s\right)-w_v\left(T\right)\right]$ (9)

- At the condenser

$$m_f c_{pf}\left(\frac{\partial T_f}{\partial t}\right)=\sum_{j=1} hc_j S_j\left(T_{j,pi}-T_f\right)+\dot{m}h_{fg} \quad (10)$$

- At the riser and downcomer level

$$m_f c_p\left(\frac{\partial T_f}{\partial t}+U\frac{T_f-T_{f-1}}{\Delta x}\right)=hcS\left(T_{pi}-T_f\right) \quad (11)$$

2.4.5 Heat transfer coefficients

The convective exchange coefficient between the external walls and the environment can be calculated by [15] :

$$hc_e=5.7+3.8\times v \quad (12)$$

The natural convection heat exchange coefficient between the vertical internal walls and the air in the habitat enclosure is determined using the correlation of Churchill and Chu [16], [17]:

$$Nu=0.68+0.67Ra^{1/4}\left\{1+\left(\frac{0.492}{\mathrm{Pr}}\right)^{9/16}\right\}^{-4/9} \quad ; \text{ avec } Ra\le 10^9 \quad (13)$$

The convective exchange coefficient between the internal air of the habitat and the horizontal walls is calculated by the correlation proposed by MacAdams [18] :

$$Nu=0.27Ra^{0,25} \quad (14)$$

The convective heat exchange coefficient between the refrigerant and the inner walls of the evaporator is calculated by [19] :

$$hc_{evap}=0.00122\left\{\frac{c_{pl}^{0.45}\rho_l^{0.49}\lambda_l^{0.79}}{\sigma_f^{0.5}h_{fg}^{0.24}\mu_l^{0.29}\rho_v^{0.24}}\Delta T_s^{0.24}\Delta P_s^{0.75}\right\} \quad (15)$$

The natural convection transfer coefficient during condensation between the fluid and the inner walls of the condenser is calculated by [20] :

$$hc_{cd} = 0.943\left\{\frac{\rho_l g \lambda_l^3 h_{fg}\left(\rho_l - \rho_v\right)}{\mu_l L_{cd}\left(T_s - T_p\right)}\right\}^{1/4} \quad (16)$$

The radiation heat exchange coefficient between two parallel rectangular walls (i and j) of the same area is calculated by the relation (17) :

$$hr_{i,j} = \frac{\sigma\left(T_i + T_j\right)\left(T_i^2 + T_j^2\right)}{\frac{1}{\varepsilon_i} + \frac{1}{\varepsilon_j} - 1} \quad (17)$$

The radiation heat exchange coefficient between two perpendicular walls with a common side is deduced from relation (18) :

$$hr_{i,j} = \sigma \varepsilon_i F_{i,j}\left(T_i + T_j\right)\left(T_i^2 + T_j^2\right) \quad (18)$$

The sky temperature is calculated by the following expression [15]:

$$T_{sky} = 0,0552\left(Ta\right)^{1,5} \quad (19)$$

2.5 Climatic conditions

In this work we use the typical day of March in the region of Mamou (Guinea). These are very hot days of the year with an average minimum temperature of about 25 °C and maximum of about 35 °C. The maximum global solar flux is 1000 W/m². The hourly variations of the solar flux and the ambient temperature are obtained from the sinusoidal functions as shown in Fig. 3.

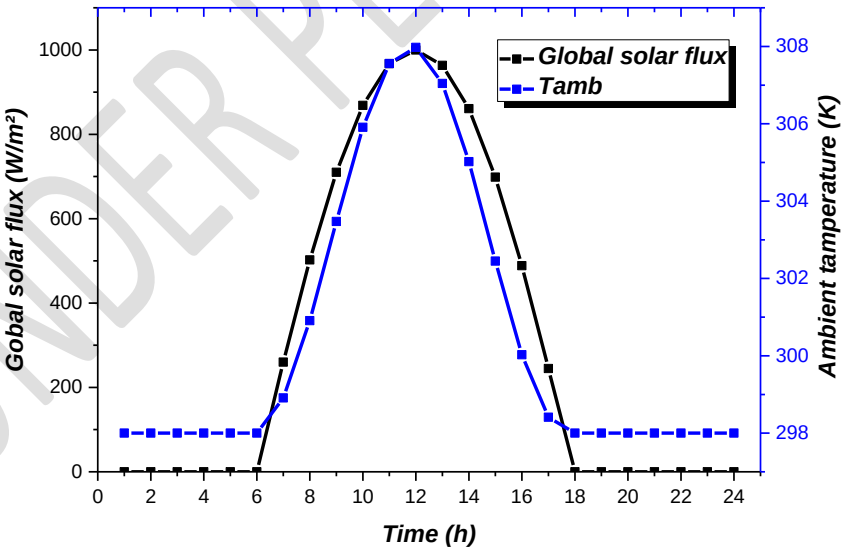

Fig. 3. Daily evolution of the horizontal global flux and the ambient temperature.

2.6 Method of numerical solution

All heat transfer balance equations have been discretized and are solved by the implicit finite difference method based on the Gauss algorithm for the housing and Thomas for the air conditioning

system. It is an iterative calculation that determines the unknown variables at time $t + \Delta t$ from the known ones at time t.

3. RESULTS AND DISCUSSION

3.1 Evolution of the solar flux density incident on the habitat

- On the roof

The slightly sloping, almost horizontal roof receives the highest solar flux and peaks at noon with a maximum value of 966.13 W/m². The solar flux incident on the roof is shown in Fig. 4.

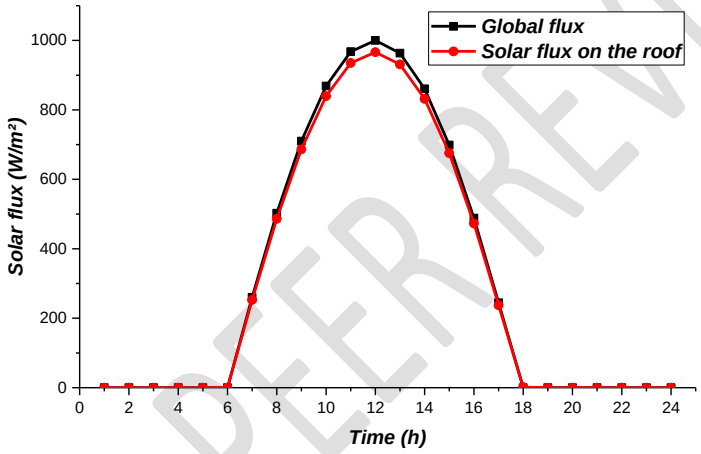

Fig. 4. Evolution of the solar flux density incident on the roof.

- At the level of the vertical walls

The temporal evolution of the incident solar flux is linked to the orientation of each wall and also to the position of the sun at each moment of the day (see Fig. 5). In this case, the most important flux arrives on the East wall with a peak at 10 am for a value of 671.93 W/m². This flux decreases progressively until 1 p.m., which corresponds to the passage of the sun from the East to the West wall. From 1 p.m., the incident flux on the west wall increases to reach a peak at 3 p.m. with a value of 495.48 W/m² and it progressively decreases until it becomes zero at 6 p.m. In addition, the radiant flux on the south wall is greater than that on the north wall. The flux arriving on the South wall reaches a peak of 368.48 W/m² and 148.67 W/m² on the North wall at 12 h.

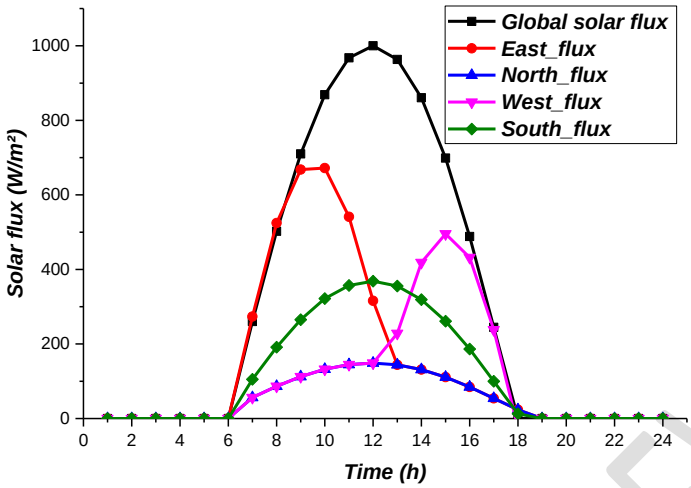

Fig. 5. Density of solar flux incident on the different vertical walls.

3.2 Model Validation

The numerical code of our model was validated by comparing our results with those obtained by Tong, Z & al [21] through an experimental study. They performed an experiment on the self-regulation performance of a two-phase thermosiphon loop with double parallel evaporators. The working fluid is the refrigerant R744, unlike our system which works with methanol. The temperature on the surface of the evaporator is measured with Pt1000 sensors. Fig. 6, shows a good qualitative agreement between our numerical simulation results and their experimental model. These results confirm the validity of the numerical code used for the simulation.

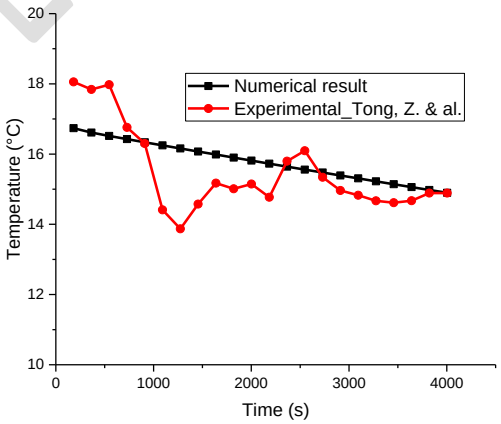

Fig. 6. Model validation from the evaporator.

In addition we validated the numerical code of the habitat from the studies performed by Camara, Y. & al. [14]. They numerically studied a one-dimensional heat transfer in a habitable enclosure in hot countries. The results presented in Fig. 7, show the evolution of temperature profiles on the external roof of our habitat model and that of Camara Y. These results are in good qualitative agreement with a similar trend of the curves of the studied model. Indeed, differences in temperature are observed between our two models. This difference is mainly due to the fact that the thermo-physical properties of the materials are different. Our model uses galvanized steel sheets and clay bricks. On the other hand, Camara Y's study concerns a habitat with an aluminium roof and stabilized earth bricks.

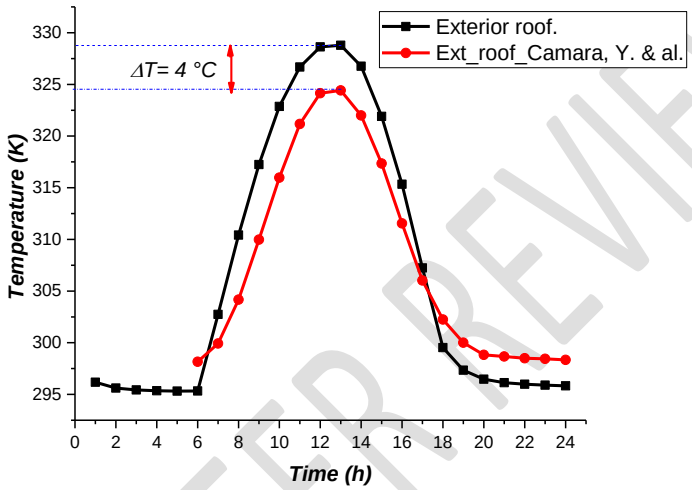

Fig. 7. Habitat model validation.

3.3 Loop temperature profile

In Fig. 8, we show the temperature profile on the evaporator walls before and after coupling the habitat. A different curve shape was observed. The shape of the curve after coupling changes compared to the curve before coupling the habitat. This change is due to the variation of the ambient air temperature in the room to be cooled. This variation has an impact on the operation of the air conditioner. On the other hand, before coupling the ambient air temperature is constant. The maximum temperature value reached on the evaporator walls is about 14 °C at 6 pm.

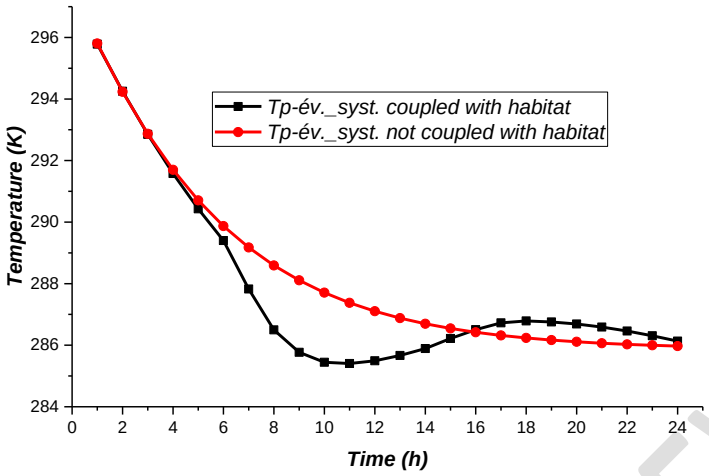

Fig. 8. Evaporator temperature profile before and after habitat coupling.

The temporal evolution of the temperature at the condenser is presented in Fig. 9. It is placed on the external East wall of the house with a surface of S=0.5 m². In the course of time, the temperature increases and reaches a peak of about 46.37°C at 14:00. This increase is mainly due to the release of heat during the condensation of the methanol vapour on the walls of the condenser and the physical phenomena of the environment (such as wind, solar flux, temperature, etc.).

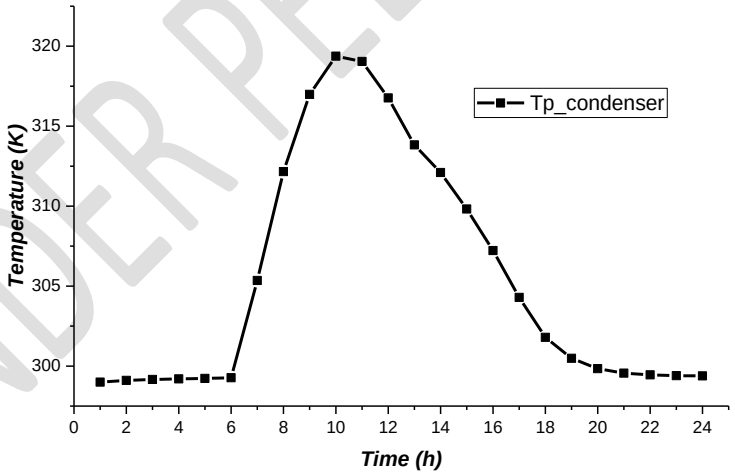

Fig. 9. Temperature evolution at the condenser.

The temporal evolution of the fluid flow rate at the condenser and evaporator is shown in Fig. 10. We can see a significant increase in the flow rate during the day and a tendency to decrease towards the evening. This is quite normal, as the operation of the air conditioner is ensured by a temperature difference between the medium to be cooled and the environment. An increase in this difference immediately leads to an increase in the flow rate in the loop. Thus, the maximum flow rate is about $2{,}71 \times 10^{-4}$ kg/s at the evaporator and $1{,}36 \times 10^{-4}$ kg/s at the condenser.

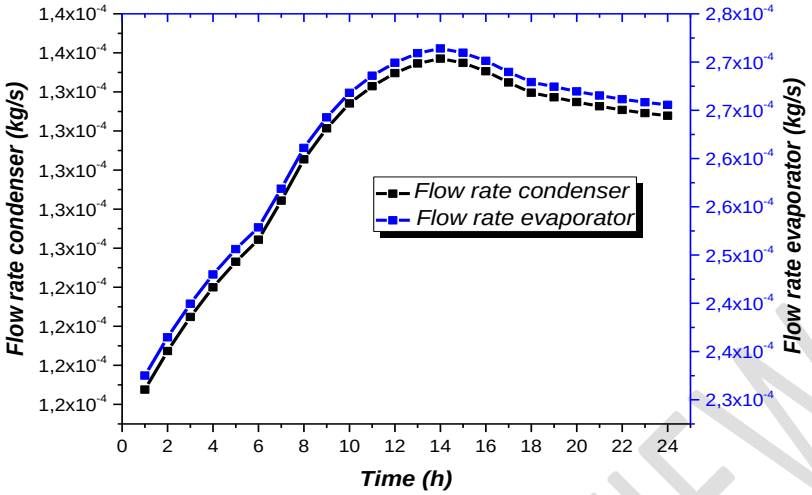

Fig. 10. Evolution of the flow rate at the condenser and evaporator.

3.4 House temperature profiles with and without air conditioning

Fig. 11. shows the evolution of the temperature profiles of the indoor air of the house before and after the coupling of the air conditioner. The numerical simulation was done with $15\ \mathrm{cm}$ wall thickness, an evaporator surface of $2\ \mathrm{m}^2$ and without air exchange. The air generates conditioner a decrease in the temperature of the living environment. This decrease is due to the convective heat exchange between the air in the room to be cooled and the air in the evaporator. The heat from the room is captured by the evaporator by evaporating the refrigerant it contains towards the condenser. The maximum temperature of the air inside the house with the air conditioner is about $26\ ℃$ à $15\ \mathrm{h}$ while the air temperature without the air conditioner is about 30°C at 3 p.m. The air conditioner reduced the ambient temperature of the living space by 4 °C.

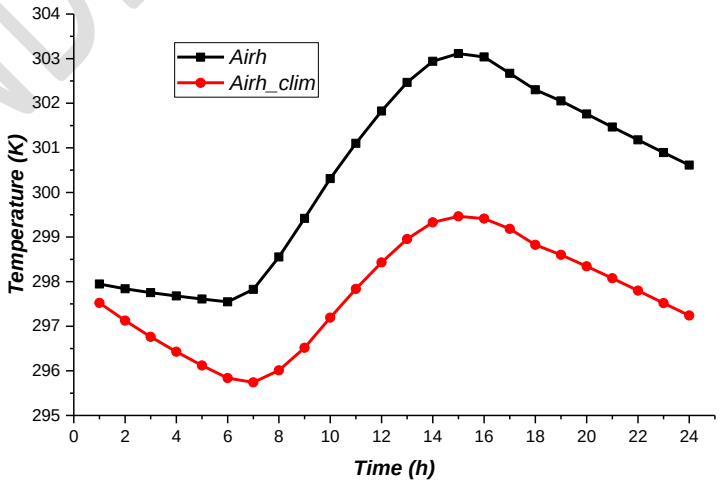

Fig. 11. Temperature profiles of indoor air with and without air conditioner.

The evolution of the temperature profiles on the internal walls of the room with and without the air conditioner is shown in Fig. 12 and Fig. 13. The following results show us the effect of the air conditioner on the temperature of each wall of the house. It lowers the temperatures on all the walls. On Fig. 12, we observe a peak of temperature at 5 p.m. whose maximum value of temperature on the East wall with the air conditioner is equal to approximately 29 °C. On the other hand, the temperature value on this wall without air conditioner is equal to 30 °C. Also on the curves of Fig. 13, the maximum temperatures of the walls with the air conditioner are observed at 14 h for the false ceiling, at 17 h for the floor whose values are respectively equal to approximately 33 °C and 27 °C. On the other hand, the temperature values for these same walls without the air conditioner are respectively 34.12 °C for the false ceiling and 28 °C for the floor.

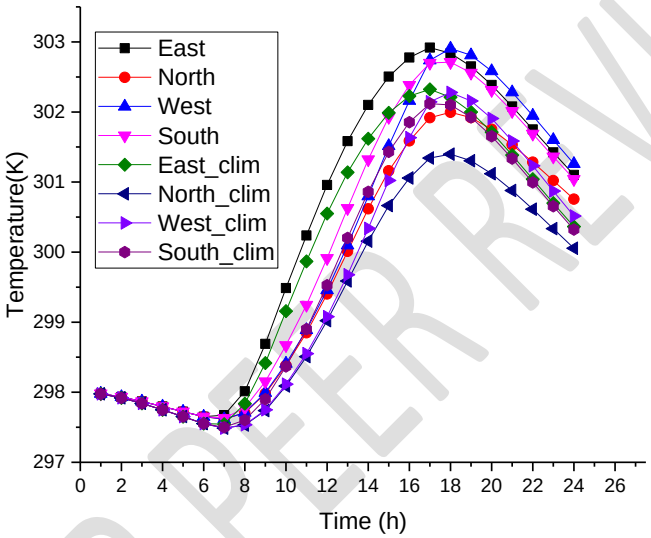

Fig. 12. Temperature profile on the internal vertical walls of the room with and without air conditioning.

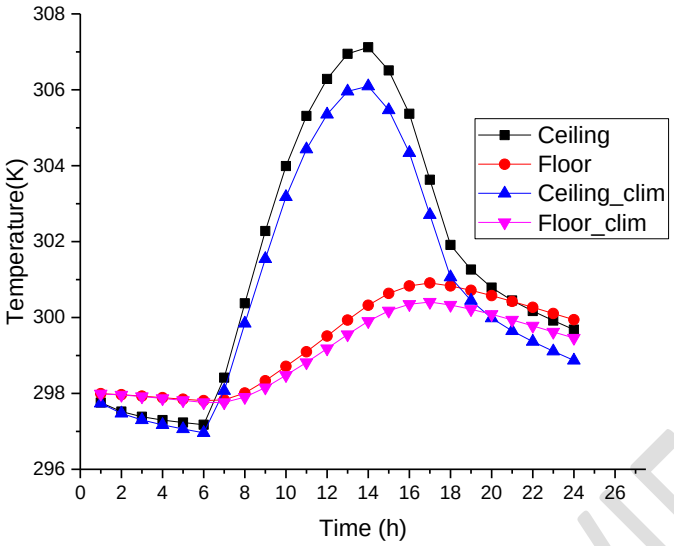

Fig. 13. Temperature profile on the internal horizontal walls of the room with and without air conditioning.

3.5 Influence of the parameters on the room air temperature

We present in Fig. 14, the effect of the thickness variation on the indoor air temperature of the habitat with the air conditioner. The variation of the thickness of the wall from 10 cm to 40 cm allowed us to observe its influence on the temperature profile of the air in the living space. We find that the temperature profiles evolve below the curve for a habitat without air conditioner. A small thickness increases the discomfort of the room. The maximum temperature values reached for a thickness of $10\ \mathrm{cm}$ and $40\ \mathrm{cm}$ are 28.5 °C and 23.9 °C respectively. However, the temperature for a house without air conditioning is 30 °C.

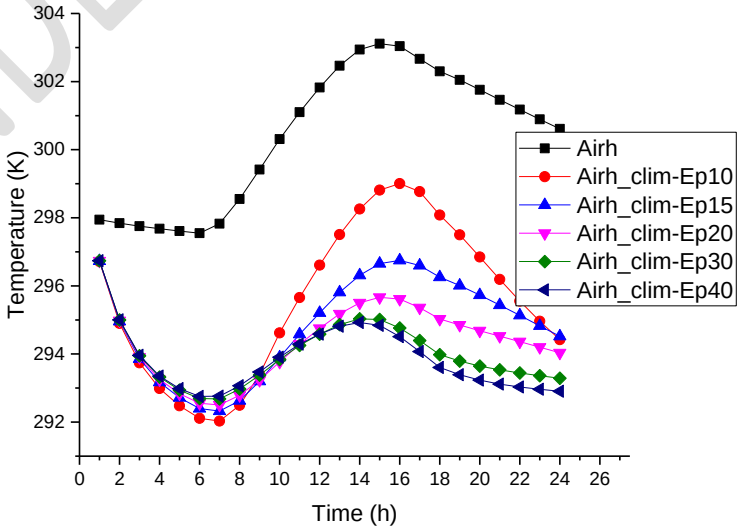

Fig. 14. Effect of wall thickness variation on indoor air temperature of the house with air conditioner.

Figure 15 also shows the effect of the variation of the air exchange rate on the temperature profile of the room coupled to the air conditioning unit. Air infiltration through open doors or windows has a negative impact on the operation of the air conditioning unit and thus leads to an increase in the air temperature in the room. At an air change rate of N=10, the maximum temperature of the room air is about 30.6 °C at 2 p.m.

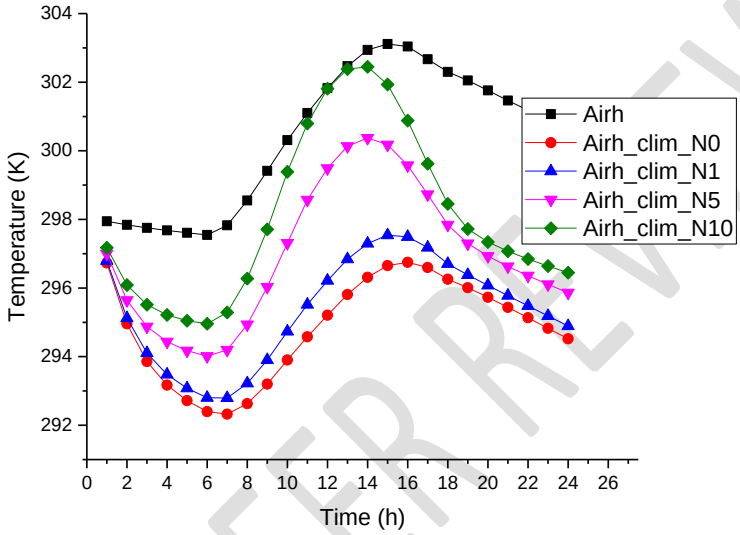

Fig. 15. Effect of the variation of the air exchange rate on the air temperature of the room equipped with the air conditioner.

We have varied the intensity of the solar flux incident on the habitat from 900 W/m² to 1500 W/m² to observe the impact of this on the cooling of the room (Fig. 16). It is obvious that solar radiation has a very important effect on cooling. The increase of the solar flux also leads to the increase of the temperature of the air-conditioned room. We can see from the curves that in the absence of the sun, the thermal load in the room is almost stable. For a maximum flux of 1500 W/m², the maximum temperature reached in the room is 28.5 °C from 3 pm.

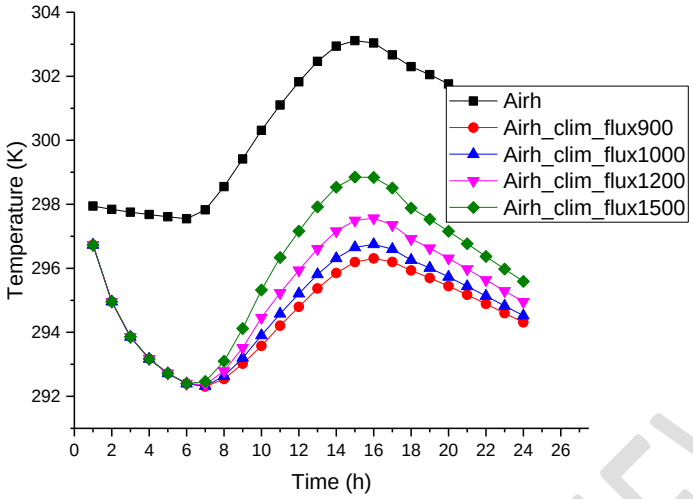

Fig. 16. Influence of the variation of the solar flux on the temperature of the air inside the room equipped with the air conditioner.

We varied the maximum ambient temperature from 35°C to 45°C (Fig. 17) and the minimum ambient temperature from 15°C to 30°C (Fig. 18) in order to observe the impact of these temperatures on the temperature of the air inside the room equipped with the air conditioner. We note that these variations have an influence on the internal temperature of the room and also on the operation of the air conditioning unit. When the temperature of the room increases, the temperature difference between the room and the environment decreases and the performance of the air conditioner decreases. This leads to an increase in the internal temperature.

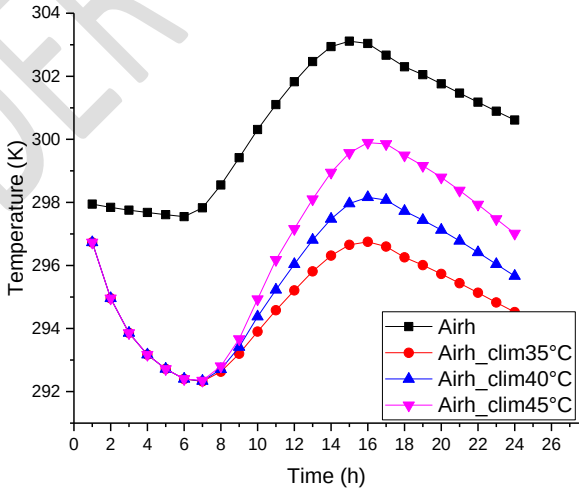

Fig. 17. Influence of the minimum temperature on the air temperature in the room with the air conditioner.

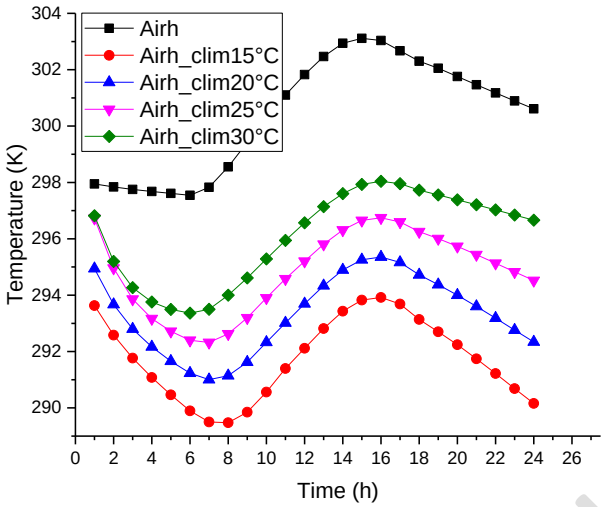

Fig. 18. Influence of the minimum temperature on the air temperature in the room with the air conditioner.

The influence of the variation of the evaporator surface on the temperature of the air inside the room is shown in Fig. 19. The simulation was carried out with a wall thickness of 15 cm, without air exchange and a maximum solar flux of 1000 W/m². We varied the surface of the evaporator from 0.5 m² to 3 m² to observe the impact of this surface on the cooling of the room. The results show that the larger the surface area, the greater the convective exchange between the air in the room and the evaporator walls, and the lower the temperature of the air inside the room. The maximum value of the temperature of the air inside the room is equal to approximately 25 °C for an evaporator surface of 3 m² and approx. 29 °C for a surface of 0.5 m².

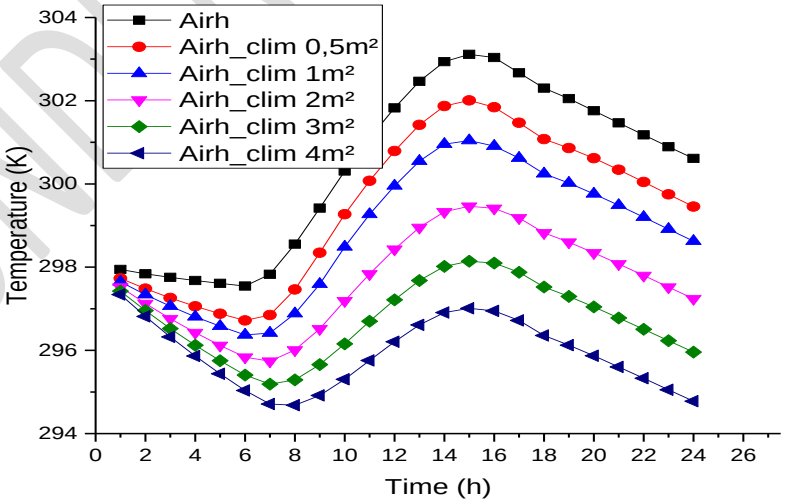

Fig. 19: Influence of the evaporator surface on the room air temperature.

4. CONCLUSION

This paper presents a numerical study of the passive air conditioning of a typical room in Guinea by a two-phase thermosiphon loop. The model was studied with meteorological data from the city of Mamou. The results showed the feasibility of this air conditioner in a dry and humid tropical (foutanian) climate. The value of the maximum temperature of the indoor air of the habitat with the air conditioner is about 26 °C while the air temperature without the air conditioner is about 30°C. Thus, the air-conditioning loop reduced the ambient temperature of the living space by 4 °C. Indeed, the larger the evaporator surface, the lower the room temperature. The variation of certain parameters also clearly showed their behaviour on the air temperature in the air-conditioned room. In general, they have a negative impact on the operation of the air conditioner and contribute to the increase of the temperature of the air conditioned room. Parameters such as air exchange, wall thickness, evaporator surface, etc. must be optimized in the design for good indoor thermal comfort. The thermosyphon loop is an alternative in passive air-conditioning of premises for cities with energy deficits or entirely without a conventional energy source.

NOMENCLATURE

c_p : Heat capacity by mass $\left(J/kg.K\right)$

DF : Solar flux density $\left(W/m^2\right)$

e : Thickness $\left(m\right)$

G_p : Incident solar flux density $\left(W/m^2\right)$

h_{xij} : Heat transfer coefficient according to the transfer mode x $\left(W/m^2.K\right)$

hc : Convective heat transfer coefficient $\left(W/m^2.K\right)$

hr : Radiation heat transfer coefficient $\left(W/m^2.K\right)$

h_{fg} : Latent heat of vaporization $\left(J/kg\right)$

L : Length $\left(m\right)$

m : Mass $\left(kg\right)$

$\dot{m}$: Mass flow rate (kg/s)

N : Air change rate $\left(h^{-1}\right)$

Nu : Nusselt number

Pr : Prandtl number

Ra : Rayleigh number

S : Surface $\left(m^2\right)$

T : Temperature $\left(K\right)$

t : Time $\left(s\right)$

U : Flow velocity $\left(m/s\right)$

V : Volume $\left(m^3\right)$

v : Wind velocity $\left(m/s\right)$

w : The mass fraction

Δx : No distance $\left(m\right)$.

Greek Symbols

α_p : The coefficient of absorptivity ;

Φ_i : Heat source or sink $\left(W/m^2\right)$

ϕ_{ra} : Air renewal $\left(W/m^2\right)$

β_m : Mass expansion coefficient $\left(K^{-1}\right)$

σ : The Stefan-Boltzmann constant $\left(5.67\times10^{-8}Wm^2K^{-4}\right)$

ε : Emissivity

ρ : Density $\left(kg/m^3\right)$

λ : Thermal conductivity $\left(W/m.K\right)$

σ_f : Surface tension $\left(N/m\right)$

μ : Dynamic viscosity $\left(kg/m.s\right)$

Indexes

a : Ambient
ai : Indoor air of the room
cd : Condenser
e : Outdoor
$evap$: Evaporator
f : Fluid
l : Liquid
M : Materials considered
pe : Exterior wall
pi : Inside wall
s : Saturation
v : Steam
vs : Saturating steam

RÉFÉRENCES

1. Bhamare, D. K., Rathod, M. K., & Banerjee, J. (2019). Passive cooling techniques for building and their applicability in different climatic zones—The state of art. Energy and Buildings, 198, 467-490.

2. Santamouris, M., Sfakianaki, A., & Pavlou, K. (2010). On the efficiency of night ventilation techniques applied to residential buildings. Energy and Buildings, 42(8), 1309-1313.

3. MEH & PNUD. (2014). Evaluation et Analyse des Gaps par rapport aux objectifs de SE4ALL, Rapport final 1. www.se4all-africa.org/fileadmin/uploads/se4all/Documents/Country_RAGAs/Guinea_RAGA_FR_Released.pdf

4. Ibrahim, E., Shao, L., & Riffat, S. B. (2003). Performance of porous ceramic evaporators for building cooling application. Energy and Buildings, 35(9), 941-949.

5. LE MASSON, S., MECHERI, B., LOUAHLIA-GUALOUS, H., & NORTERSHAUSER, D. Boucle diphasique à minicanaux pour le refroidissement de cartes de télécommunication.

6. Franco, A., & Filippeschi, S. (2013). Experimental analysis of closed loop two phase thermosyphon (CLTPT) for energy systems. Experimental thermal and fluid science, 51, 302-311.

7. Mecheri, B. (2011). Refroidissement d'une armoire de Télécommunication avec Bouche Diphasique Thermosyphon (Thèse de doctorat, Belfort-Montbéliard).

8. Chehade, A., Louahlia-Gualous, H., Le Masson, S., & Lépinasse, E. (2015). Experimental investigations and modeling of a loop thermosyphon for cooling with zero electrical consumption. Applied Thermal Engineering, 87, 559-573.

9. Cao, H., Ding, T., He, Z., & Li, Z. (2018). Recherche sur la hauteur de colonne de fluide frigorigène dans le déversoir d'un thermosiphon à boucle diphasique. Journal international de la réfrigération, 94, 40-48.

10. Zhang, P., Wang, B., Shi, W., Han, L. et Li, X. (2015). Modélisation et analyse des performances d'une boucle thermosiphon diphasique avec déversoir partiellement/entièrement rempli de liquide. Revue internationale du froid, 58, 172-185.

11. Khodabandeh, R., & Furberg, R. (2010). Heat transfer, flow regime and instability of a nano-and micro-porous structure evaporator in a two-phase thermosyphon loop. International journal of thermal sciences, 49(7), 1183-1192.

12. Tong, Z., Liu, X. H., Li, Z., & Jiang, Y. (2016). Experimental study on the effect of fill ratio on an R744 two-phase thermosyphon loop. Applied Thermal Engineering, 99, 302-312.

13. Tong, Z., Ding, T., Li, Z., & Liu, X. H. (2015). An experimental investigation of an R744 two-phase thermosyphon loop used to cool a data center. Applied Thermal Engineering, 90, 362-365.

14. Camara, Y., Chesneau, X., & Kante, C. (2018). Etude numérique du confort thermique dans un habitat bioclimatique en brique de terre stabilisée pour un climat type de la Guinée. Afrique Science, 14(2), 238-254.

15. Oudrane, A., Aour, B., Zeghmati, B., Chesneau, X., & Hamouda, M. (2017). 'Analyse numérique du transfert de chaleur unidimensionnel pour la maison du désert. Recueil de mécanique, 2 (01), 089-102.

16. Khalifa, A. J. N. (2001). Natural convective heat transfer coefficient–a review: I. Isolated vertical and horizontal surfaces. Energy conversion and management, 42(4), 491-504.

17. Churchill, S. W., & Chu, H. H. (1975). Correlating equations for laminar and turbulent free convection from a vertical plate. International journal of heat and mass transfer, 18(11), 1323-1329.

18. Camara, Y. (2018). Etude numérique des performances thermiques d'un habitat bioclimatique (Doctoral dissertation, Perpignan).

19. Salem, M. A. M. (2010). Experimental study for transient response of a double-tube thermosyphon (DTTH).

20. Naresh, Y., & Balaji, C. (2018). Thermal performance of an internally finned two phase closed thermosyphon with refrigerant R134a: A combined experimental and numerical study. International Journal of Thermal Sciences, 126, 281-293.

21. Tong, Z., Liu, X. H., & Jiang, Y. (2017). Experimental study of the self-regulating performance of an R744 two-phase thermosyphon loop. Applied energy, 186, 1-12.